Improved Control of BLDCM Considering Commutation Torque Ripple and Commutation Time in Full Speed Range

Weidong Jiang, *Member, IEEE*, Yuming Liao, Jinping Wang, *Member, IEEE*, Peixia Wang, and Yifan Xie

***Abstract*—The three phases of brushless dc motor (BLDCM) are involved in energy conversion during the commutation interval. A novel commutation analysis method of the BLDCM based on coordinate transformation theory is proposed in this paper, though this coordinate transformation theory is popular in the control of three-phase sinusoidal motors, such as induction motors and permanent magnet synchronous motors. The method is intuitive and easy to understand compared with the method based on circuit solving. Combined with the voltage vector diagram of the inverter, commutation control to reduce commutation torque ripple under low speed (LS_RCTR) and high speed (HS_RCTR) is deduced. However, under a heavy load and high-speed condition, long commutation time may result in commutation failure if these commutation controls to RCTR is adopted. To avoid that, commutation time must be controlled. Then, commutation control to reduce commutation time under low-speed (LS_RCT) and high-speed (two cases, named HS_RCT1 and HS_RCT2) are proposed. The improved control of BLDCM presented in this paper can coordinate commutation torque ripple and commutation time in full speed range. Finally, the feasibility and effectiveness of these methods are verified by experiment.**

***Index Terms*—Brushless dc motor (BLDCM), commutation time, commutation, torque ripple.**

I. Introduction

THE brushless dc motor (BLDCM), with a trapezoidal back electromotive force (EMF) waveform, is widely used in robotics, aerospace, automotive, household appliances, and medical applications because of its highly desirable features, such as a high torque/weight ratio, high efficiency, low maintenance, longer life span, and easy-to-drive features [1]–[3].

However, torque ripple has always been a major and passive factor preventing BLDCMs from achieving higher performance.

Manuscript received August 30, 2016; revised December 1, 2016, February 20, 2017, April 1, 2017, and May 23, 2017; accepted June 13, 2017. Date of publication June 20, 2017; date of current version February 1, 2018. This work was supported by the National Natural Science Foundation of China under Grant 51407054 and Grant 51177037. Recommended for publication by Associate Editor B.G Fernandes. *(Corresponding Author: Weidong Jiang.)*

The authors are with the School of Electrical Engineering and Automation, Hefei University of technology, Hefei 230009 Chinaand also with the Department of Information Engineering, Hefei University of Technology (Xuancheng Campus), Xuancheng 242000, China (e-mail: ahjwd@163.com; 18726382359@163.com; waupter919@163.com; 1565482534@qq.com; 948854654@qq.com).

Color versions of one or more of the figures in this paper are available online at http://ieeexplore.ieee.org.

Digital Object Identifier 10.1109/TPEL.2017.2717484

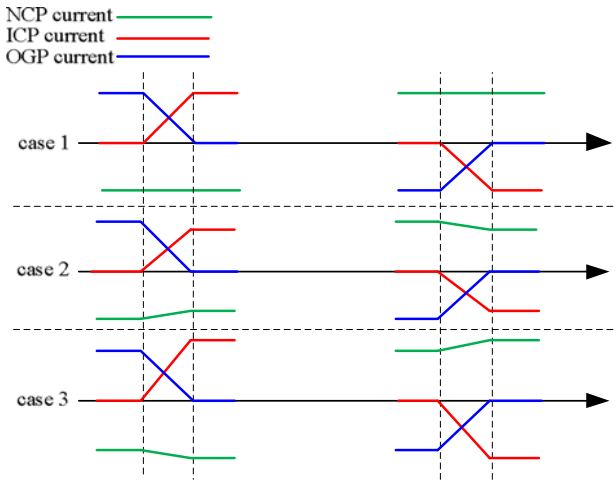

Fig. 1. Typical three-phase currents during commutation interval.

The main reasons causing torque ripple in BLDCMs are as follows:

1) the imperfection of the motor design and manufacture, including nonideal EMFs [4]–[6];

2) the pulse width modulation (PWM) causes a small but high-frequency torque ripple;

3) commutation torque ripple causes a worse effect, even leading to a significant torque ripple up to 50% of the average torque.

The commutation torque ripple is serious because it is sudden and strong. Much research has focused on this problem [7]–[20]. In fact, this paper also deals with commutation torque ripple and the related issues.

The theoretical derivation of commutation torque ripple was first given in [7] by R. Carlson. In [7], [8], the difference between the current slew rates of the incoming phase (ICP) and the outgoing phase (OGP) is considered as the main reason for commutation torque ripple. Fig. 1 shows three typical cases of the phase currents during the commutation interval. The commutation torque ripple is not presented under case 1, and it takes place under cases 2 and 3.

Case 1: The decrease rate of the OGP is equal to the increase rate of the ICP, and the noncommutation phase (NCP) current does not vary during the commutation interval.

Case 2: The decrease rate of the OGP is greater than the increase rate of the ICP, and the NCP current decreases during the commutation interval.

Case 3: The decrease rate of the OGP is smaller than the increase rate of the ICP, and the NCP current increases during the commutation interval.

Many methods have been proposed to reduce commutation torque ripple (RCTR). These methods can be divided into two categories. The first uses various PWM. In this category, the classical three-phase bridge is used, usually with constant dc voltage. The second uses an adjustable dc–dc converter to keep the dc-link voltage four times larger than that of the phase back EMF. And an extra front converter is needed in this method.

The overlapped commutation method is presented in [9], in which the OGP is modulated during the commutation interval over full speed range. In [10], [11], a method to minimize commutation torque ripple was presented and developed. In the method, the ICP is on, whereas both the OGP and the NCP are modulated with the same duty cycle during commutation interval. The basic idea is to reduce the current slew rate of the faster one between ICP and OGP, so as to keep the NCP current constant. In [13], a novel three-segment modulation method is proposed to suppress commutation torque ripple, which is realized by modifying the duty ratio according to the voltage of the NCP before commutation and keeping the average voltage of the NCP constant during commutation interval. According to the value function, the optimal vector is selected during commutation interval in [14].

Another category of methods to RCTR uses an adjustable dc–dc converter to control the dc-link voltage. In [15]–[17], an adjustable dc–dc converter was applied to maintain the dc-link voltage four times larger than that of the phase back EMF, because the current slew rates of ICP and OGP can be the same. This method is very dependent on the dynamic response of the dc–dc converter. In [18], a novel topology is proposed to RCTR in a BLDCM drive system using a three-level neutral-point-clamped inverter combined with single-ended primary-inductor converter. In [19], a single-phase supply followed by a diode bridge rectifier and a modified-zeta converter that operates in discontinuous conduction mode is used to feed a voltage source inverter (VSI). The modified-zeta converter acts as an inherent power factor preregulator. In [20], a novel commutation torque ripple reduction strategy for BLDCM-based zeta-source converter is proposed. The proposed strategy employs the same modulation mode during both commutation interval and non-commutation interval, and the commutation torque ripple is reduced by regulating the duty cycles of shoot-through vector and active vector.

If the dc-link is acquired by an uncontrolled rectifier from three-phase 380-V ac grid, the dc-link voltage is 500–537 V. The switch device with 1200-V rated voltage can be used without a dc–dc converter. If a dc–dc converter is applied to maintain the dc-link voltage four times larger than that of the phase back EMF, considering the full speed range of BLDCM, a switch device with more than 1500-V rated voltage must be used to meet the requirement of voltage stress. Thus, the dc–dc converter is not a good candidate because of cost, efficiency, and reliability.

With the pursuit of high speed, high power density, and high electrical frequency, large phase inductance, and finite dc-link voltage becomes the limiting factors, and then a long commutation may emerge during nominal operation [21]–[23]. Apart from the commutation torque ripple, the commutation time must be considered to avoid commutation failure.

The commutation time is directly determined by two factors: 1) the energy stored in the OGP, which is determined by the phase inductance and phase current of the OGP; and 2) the discharge rate, which is determined by the dc-link voltage, EMF, and commutation control method. In [24], a rigorous analytic investigation, instead of the conventional analysis, is presented, where all six factors influencing the commutation time in a BLDCM drive system are identified and analyzed in detail. Another contribution of the work in [24] is the revelation that finite dc-link voltage is an important reason causing a long commutation time.

Since finite dc-link voltage is an important reason for long commutation, a higher voltage should be provided to shorten the commutation time. It is worth pointing out that, although the commutation process can also be regulated using various PWM methods when the dc-link voltage remains constant [9]–[14], the commutation time is rarely shortened. Even if a novel three-segment modulation method is proposed to obtain the minimum commutation time [13], when the duty cycle is close to 1, the commutation time is still very long.

During the commutation interval, the three-phase voltages should be controlled simultaneously. There are three different equations that need to be solved. The analysis and solution is complex and tedious. Therefore, the number of the equations must be decreased to simplify the analysis.

The Clarke transformation is popular in the control of a three-phase sinusoidal motor, such as an induction motor and permanent magnet synchronous motor. But it has not been used in the commutation control of BLDCM. By introducing the Clarke transformation into the commutation analysis, some intuitive control strategies, and conclusions can be acquired.

In fact, a three-phase VSI feeds the BLDCM with star connection. There are only two independent control variables from the viewpoint of the VSI. Therefore, coordinate transformation is needed to reduce the number of control variables very naturally to simplify the analysis.

With the help of coordinate transformation theory, the commutation model of the BLDCM is acquired in the two-phase stationary frame and the commutation process is analyzed in detail in this paper. Combined with the voltage vector diagram of the VSI, the method to RCTR under low-speed (LS_RCTR) and high-speed (HS_RCTR) operations are acquired. To avoid commutation failure caused by heavy load and high speed, the commutation control method to reduce the commutation time is proposed under low-speed (LS_RCT) and high-speed (two cases, named HS_RCT1 and HS_RCT2).

This paper is organized as follows. Section II describes the model of the BLDCM. Commutation analysis of the BLDCM is given in Section III. The control method to RCTR is depicted in detail in Section IV. The control method to RCT is discussed in detail in Section V. Section VI introduces the hybrid

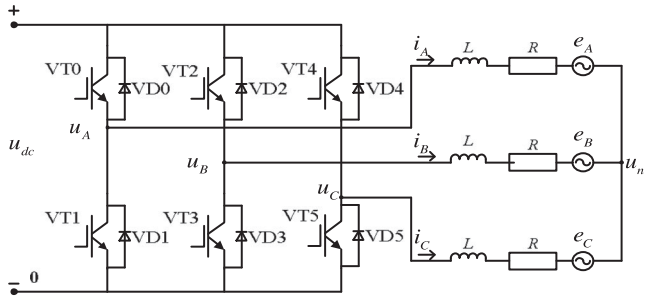

Fig. 2. Equivalent circuit of BLDCM and the inverter.

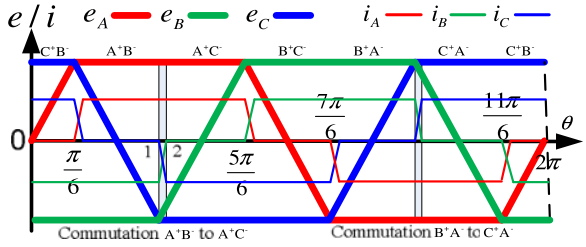

Fig. 3. Ideal waveforms of the EMFs and the phase currents of the BLDCM.

control of RCTR and RCT. Section VII verifies the outstanding features of the proposed control by means of experimental results. The conclusion is drawn in Section VIII.

II. Mathematical Model of BLDCM

A. Terminal Voltage Equation of BLDCM

The equivalent circuit of the BLDCM and its driver is shown in Fig. 2. Using the negative bus of the dc-link as the reference point, the voltage equations of the three-phase stator windings can be expressed as

$$L\frac{di_z}{dt} = -Ri_z + u_z - e_z - u_n \tag{1}$$

where $e_z, u_z, i_z (z = A, B, C)$ are the EMFs, phase voltages, and phase currents, respectively; *R* and *L* are the resistance and inductance of the phase winding; u_n and $u_{\rm dc}$ are the neutral point voltage and dc-link voltage; $u_z = d_z u_{\rm dc}$, d_z is the duty cycle of phase z.

In this paper, the analysis is focused on the PWM/ON scheme. In the scheme, the upper switch of one phase is modulated and the lower switch of another phase is ON. For example, A^+B^- represents that the windings of phase A and phase B are energized, and the upper switch of phase A (VT0) is modulated and the lower switch of phase B (VT3) is ON. The commutation from A^+B^- to A^+C^- is taken as an example of the commutation between the lower switches (LSC), and the commutation from B^+A^- to C^+A^- is taken as an example of the commutation between the upper switches (USC). In these two examples, phase *C* is ICP, phase *B* is OGP, and phase *A* is NCP.

Only two phases are involved in energy conversion during the noncommutation interval. The phase voltage equations during A^+B^- are given as

$$\begin{cases} L\dfrac{di_A}{dt} = -Ri_A + u_A - e_A - u_n \\ L\dfrac{di_B}{dt} = -Ri_B + u_B - e_B - u_n \end{cases}. \tag{2}$$

In the PWM/ON scheme, the LSC of phase *B* is ON, so $u_B = 0$; and the USC of phase *A* is modulated with the duty cycle of $d_{\rm NC}$, then $u_A = d_{\rm NC}u_{\rm dc}$. Considering that $i_B = -i_A$, formula (2) can be simplified as

$$d_{\rm NC}u_{\rm dc} - 0 = 2Ri_A + 2L\frac{di_A}{dt} + (e_A - e_B). \tag{3}$$

In the stable state of the BLDCM, it can be found that the phase EMFs $e_A = E$ and $e_B = -E$ during A^+B^- from Fig. 3, where E denotes the EMF. From (3), the relation between the EMFs and the phase voltage can be obtained as

$$E = e_A = -e_B = \frac{d_{\rm NC}u_{\rm dc} - 2Ri_A}{2}. \tag{4}$$

B. Electromagnetic Torque Equation

The electromagnetic torque $T_{\rm em}$ is given as

$$T_{\rm em} = \frac{p_{\rm em}}{\omega} = \frac{\sum_{z=A,B,C} e_z i_z}{\omega} \tag{5}$$

where ω is the angular velocity of the BLDCM. During the commutation interval, the total electromagnetic power $p_{\rm em}$ is the sum of the three phases' electromagnetic power. Similarly, it represents the sum of the two energized phases' electromagnetic power during the noncommutation interval. So, to maintain torque constant, constant electromagnetic power should be achieved.

III. Commutation Analysis in the Two-Phase Stationary Frame

The transformation expressions with equal power from the three-phase ABC stationary frame to the two-phase stationary frame can be expressed as

$$\mathbf{x} = x_\alpha + jx_\beta = \sqrt{2/3}(x_A + x_B e^{j120^\circ} + x_C e^{j240^\circ}) \tag{6}$$

where x_α and x_β denote the α- and β-axis components of vector **x**, respectively. The transformation given by (6) is well known as the Clarke transformation, which is popular in the control of three-phase sinusoidal motors, such as induction motors and permanent magnet synchronous motors. But it has not been used in the commutation control of BLDCM. By introducing the Clarke transformation into the commutation control of the BLDCM, some intuitive control strategies and conclusions can be acquired.

Combining (6) and (1), the terminal voltage equations of BLDCMs in the two-phase stationary frame during the commutation interval can be expressed as

$$L\frac{di_{\alpha,\beta\rm CI}}{dt} = u_{\alpha,\beta\rm CI} - Ri_{\alpha,\beta\rm CI} - e_{\alpha,\beta\rm CI} \tag{7}$$

where $i_{\alpha,\beta\rm CI}$, , $e_{\alpha,\beta\rm CI}$, and $u_{\alpha,\beta\rm CI}$, respectively, denote the α- and β-axis components of the current vector, the EMF vector and the voltage vector during the commutation interval.

The commutation from A^+B^- to A^+C^- is chosen as an example to analyze the commutation process in detail, and the other cases can be analyzed similarly. During the commutation interval, the EMFs assume as $e_A = -e_C = E,\ e_B \approx -E$, which is widely applied in the commutation analysis of BLDCM [9], [13], [14], [18], [28]. Combining the assumption with (4) and (6), $e_{\alpha,\beta\mathrm{CI}}$ can be obtained as

$$\begin{cases} e_{\alpha\mathrm{CI}} \approx \sqrt{2/3}(d_{\mathrm{NC}}u_{\mathrm{dc}} - 2Ri_{\mathrm{ACS}}) \\ e_{\beta\mathrm{CI}} \approx 0 \end{cases}. \tag{8}$$

Assuming i_{ACS}, i_{BCS}, and i_{CCS} denote instantaneous three-phase currents at the beginning of the commutation, respectively, then we can get $i_{\mathrm{ACS}} = -i_{\mathrm{BCS}},\ i_{\mathrm{CCS}} = 0$. Taking that into (6), the initial value of (7) can be written as

$$\begin{cases} i_{\alpha\mathrm{CS}} = \sqrt{3/2}i_{\mathrm{ACS}} \\ i_{\beta\mathrm{CS}} = \sqrt{1/2}i_{\mathrm{BCS}} = -\sqrt{1/2}i_{\mathrm{ACS}} \end{cases} \tag{9}$$

where $i_{\alpha\mathrm{CS}}$ and $i_{\beta\mathrm{CS}}$ denote the α- and β-axis components of the current vector at the beginning of the commutation. The special solution of (7) is given as

$$\begin{cases} i_{\alpha\mathrm{CI}} = \dfrac{u_{\alpha\mathrm{CI}} - e_{\alpha\mathrm{CI}}}{R}\left(1 - e^{-\frac{R}{L}t}\right) + i_{\alpha\mathrm{CS}}e^{-\frac{R}{L}t} \\ i_{\beta\mathrm{CI}} = \dfrac{u_{\beta\mathrm{CI}} - e_{\beta\mathrm{CI}}}{R}\left(1 - e^{-\frac{R}{L}t}\right) + i_{\beta\mathrm{CS}}e^{-\frac{R}{L}t} \end{cases}. \tag{10}$$

When $Rt/L \ll 1$, $e^{-Rt/L} \approx 1 - Rt/L$ is satisfied [25]. The assumption is more suitable for a slotted motor; the slotless motor should use a higher order Taylor polynomial, which is not discussed in this paper. So the special solution of (7) can be approximated as

$$\begin{cases} i_{\alpha\mathrm{CI}} \approx \dfrac{u_{\alpha\mathrm{CI}} - e_{\alpha\mathrm{CI}} - \sqrt{3/2}Ri_{\mathrm{ACS}}}{L}t + \sqrt{3/2}i_{\mathrm{ACS}} \\ i_{\beta\mathrm{CI}} \approx \dfrac{u_{\beta\mathrm{CI}} - e_{\beta\mathrm{CI}} + \sqrt{1/2}Ri_{\mathrm{ACS}}}{L}t - \sqrt{1/2}i_{\mathrm{ACS}} \end{cases}. \tag{11}$$

Assuming i_{ACE}, i_{BCE}, i_{CCE} denote the instantaneous three-phase currents at the end of the commutation, respectively, then we can get $i_{\mathrm{ACE}} = -i_{\mathrm{CCE}}$, $i_{\mathrm{BCE}} = 0$. Assuming $i_{\alpha\mathrm{CE}}$ and $i_{\beta\mathrm{CE}}$ denote the α- and β-axis components of the current vector at the end of the commutation. The relationship between $i_{\alpha\mathrm{CE}}$ and $i_{\beta\mathrm{CE}}$ can be expressed as

$$\sqrt{3}i_{\beta\mathrm{CE}} = i_{\alpha\mathrm{CE}}. \tag{12}$$

Combining (8), (11), and (12), the commutation time t_{com} can be obtained as

$$\begin{aligned} t_{\mathrm{com}} &\approx \frac{\sqrt{6}Li_{\mathrm{ACS}}}{\sqrt{3}(u_{\beta\mathrm{CI}} - e_{\beta\mathrm{CI}}) - (u_{\alpha\mathrm{CI}} - e_{\alpha\mathrm{CI}}) + \sqrt{6}Ri_{\mathrm{ACS}}} \\ &\approx \frac{6Li_{\mathrm{ACS}}}{3\sqrt{2}u_{\beta\mathrm{CI}} - \sqrt{6}u_{\alpha\mathrm{CI}} + 2d_{\mathrm{NC}}u_{\mathrm{dc}} + 2Ri_{\mathrm{ACS}}}. \end{aligned} \tag{13}$$

It can be seen that the commutation time is determined by several factors: resistance, inductance, phase currents, duty cycle during the noncommutation interval and the work point of BLDCM (corresponding to different $u_{\alpha\mathrm{CI}}$ and $u_{\beta\mathrm{CI}}$). In fact, the commutation control method, which determines the work point, is the key factor influencing the commutation time. Substituting (13) into (11), $i_{\alpha\mathrm{CE}}$ and $i_{\beta\mathrm{CE}}$ can be rewritten as

$$\begin{cases} i_{\alpha\mathrm{CE}} \approx \dfrac{\sqrt{3/2}i_{\mathrm{ACS}}[\sqrt{3}(u_{\beta\mathrm{CI}} - e_{\beta\mathrm{CI}}) + (u_{\alpha\mathrm{CI}} - e_{\alpha\mathrm{CI}})]}{\sqrt{3}(u_{\beta\mathrm{CI}} - e_{\beta\mathrm{CI}}) - (u_{\alpha\mathrm{CI}} - e_{\alpha\mathrm{CI}}) + \sqrt{6}Ri_{\mathrm{ACS}}} \\ i_{\beta\mathrm{CE}} \approx \dfrac{\sqrt{1/2}i_{\mathrm{ACS}}[\sqrt{3}(u_{\beta\mathrm{CI}} - e_{\beta\mathrm{CI}}) + (u_{\alpha\mathrm{CI}} - e_{\alpha\mathrm{CI}})]}{\sqrt{3}(u_{\beta\mathrm{CI}} - e_{\beta\mathrm{CI}}) - (u_{\alpha\mathrm{CI}} - e_{\alpha\mathrm{CI}}) + \sqrt{6}Ri_{\mathrm{ACS}}} \end{cases}. \tag{14}$$

Then, the instantaneous values of three-phase currents at the end of the commutation can be expressed as

$$\begin{cases} i_{\mathrm{ACE}} = -i_{\mathrm{CCE}} \\ \qquad \approx \dfrac{i_{\mathrm{ACS}}[\sqrt{3}(u_{\beta\mathrm{CI}} - e_{\beta\mathrm{CI}}) + (u_{\alpha\mathrm{CI}} - e_{\alpha\mathrm{CI}})]}{\sqrt{3}(u_{\beta\mathrm{CI}} - e_{\beta\mathrm{CI}}) - (u_{\alpha\mathrm{CI}} - e_{\alpha\mathrm{CI}}) + \sqrt{6}Ri_{\mathrm{ACS}}} \\ i_{\mathrm{BCE}} = 0 \end{cases}. \tag{15}$$

According to (13), the commutation time can be reduced by increasing $u_{\beta\mathrm{CI}}$ or decreasing $u_{\alpha\mathrm{CI}}$. It can be implemented by changing the work point.

The electromagnetic power p_{em} is the dot product of the EMF vector and current vector in the two-phase stationary frame. Because $e_{\beta\mathrm{CI}} \approx 0$ from (8), it can be expressed as

$$p_{em} = \mathbf{e} \cdot \mathbf{i} = e_{\alpha\mathrm{CI}}i_{\alpha\mathrm{CI}} + e_{\beta\mathrm{CI}}i_{\beta\mathrm{CI}} \approx e_{\alpha\mathrm{CI}}i_{\alpha\mathrm{CI}}. \tag{16}$$

From the analysis given above, two conclusions can be drawn.

Conclusion I: During the commutation interval, because $e_{\alpha\mathrm{CI}}$ is invariant, $i_{\alpha\mathrm{CI}}$ should be also invariant to RCTR. From (11), to make $i_{\alpha\mathrm{CI}}$ constant, $u_{\alpha\mathrm{CI}} = e_{\alpha\mathrm{CI}} + Ri_{\alpha\mathrm{CS}}$ should be satisfied. This is the basic idea for RCTR.

Conclusion II: When RCTR is introduced, the commutation time is determined by $u_{\beta\mathrm{CI}}$ and $Ri_{\alpha\mathrm{CS}}$. In some conditions, the commutation time would be long, maybe causing commutation failure. Then, RCT becomes critical, and it should be prior to RCTR.

TABLE I
COORDINATES OF THE INTRINSIC VOLTAGE VECTORS

Voltage vector	α-axis	β-axis	Voltage vector	α-axis	β-axis
000	0	0	011	$-\sqrt{2/3}u_{\mathrm{dc}}$	0
100	$\sqrt{2/3}u_{\mathrm{dc}}$	0	001	$-\sqrt{1/6}u_{\mathrm{dc}}$	$-\sqrt{1/2}u_{\mathrm{dc}}$
110	$\sqrt{1/6}u_{\mathrm{dc}}$	$\sqrt{1/2}u_{\mathrm{dc}}$	101	$\sqrt{1/6}u_{\mathrm{dc}}$	$-\sqrt{1/2}u_{\mathrm{dc}}$
010	$-\sqrt{1/6}u_{\mathrm{dc}}$	$\sqrt{1/2}u_{\mathrm{dc}}$	111	0	0

III. REDUCE COMMUTATION TORQUE RIPPLE

The BLDCM is fed by the VSI. The number of voltage vectors outputted by the VSI is eight. The coordinates of the voltage vectors can be acquired according to (6), which is listed in Table I.

The principle of RCTR is to keep the current slew rate of the OGP equal to that of the ICP, and the current of the NCP should not vary during the commutation interval. In the two-phase stationary frame, to implement RCTR, conclusion I should be

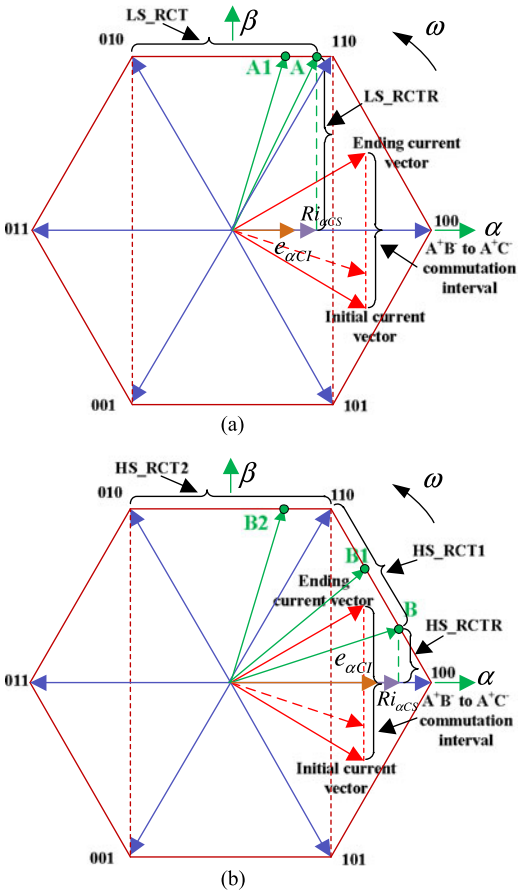

Fig. 4. Work point of VSI during the commutation interval. (a) Low-speed operation. (b) High-speed operation.

satisfied, i.e.

$$u_{\alpha \mathrm{CI}} - e_{\alpha \mathrm{CI}} - Ri_{\alpha \mathrm{CS}} = 0. \tag{17}$$

The work point of the BLDCM can be classified as two categories. One is $|e_{\alpha \mathrm{CI}} + Ri_{\alpha \mathrm{CS}}| \le \sqrt{1/6}u_{\mathrm{dc}}$, which is also expressed as $d_{\mathrm{NC}} \le \frac{1}{2} + \frac{Ri_{\mathrm{ACS}}}{2u_{\mathrm{dc}}}$ or $E \le \frac{1}{4}u_{\mathrm{dc}} - \frac{3}{4}Ri_{\mathrm{ACS}}$. The other is $|e_{\alpha \mathrm{CI}} + Ri_{\alpha \mathrm{CS}}| > \sqrt{1/6}u_{\mathrm{dc}}$, which is also expressed as $d_{\mathrm{NC}} > \frac{1}{2} + \frac{Ri_{\mathrm{ACS}}}{2u_{\mathrm{dc}}}$ or $E > \frac{1}{4}u_{\mathrm{dc}} - \frac{3}{4}Ri_{\mathrm{ACS}}$. The former is called as low-speed operation and latter is called as high-speed operation. The classification is widely used in BLDCM [10], [13], [16], [17], [26], [28].

A. LS_RCTR

As shown in Fig. 4(a), at low-speed operation, $|e_{\alpha \mathrm{CI}} + Ri_{\alpha \mathrm{CS}}| \le \sqrt{1/6}u_{\mathrm{dc}}$, in order to reduce the commutation torque ripple, $u_{\alpha \mathrm{CI}} - e_{\alpha \mathrm{CI}} - Ri_{\alpha \mathrm{CS}} = 0$ should be satisfied according to (17). $u_{\beta \mathrm{CI}}$ can vary from 0 to $\sqrt{1/2}u_{\mathrm{dc}}$. From (13), lager $u_{\beta \mathrm{CI}}$ results in shorter commutation time. So the work point of VSI is selected as *A* in Fig. 4(a).

In Fig. 4(a), for the commutation interval from A^+B^- to A^+C^-, at the beginning of the commutation $i_{\mathrm{ACS}} = -i_{\mathrm{BCS}}, i_{\mathrm{CCS}} = 0$, combining (6), the initial current vector can be obtained. At the end of the commutation, $i_{\mathrm{ACE}} = -i_{\mathrm{CCE}}, i_{\mathrm{BCE}} = 0$, combining (6), the ending current vector can be achieved. When the work point locates A, its coordinates can be expressed as

$$u_{\alpha \mathrm{CI}} + ju_{\beta \mathrm{CI}} = e_{\alpha \mathrm{CI}} + Ri_{\alpha \mathrm{CS}} + j\sqrt{1/2}u_{\mathrm{dc}} = \sqrt{2/3}d_{\mathrm{NC}}u_{\mathrm{dc}} + (\sqrt{3/2} - 2\sqrt{2/3})Ri_{\mathrm{ACS}} + j\sqrt{1/2}u_{\mathrm{dc}}. \tag{18}$$

According to the coordinates of the intrinsic voltage vectors in Table I, it can be known that the output voltage vector corresponding to point A is obtained by linear combination of voltage vectors [010] and [110]. Due to the actions of the two voltage vectors, the initial current vector moves toward the ending current vector. When the current vector reaches the ending current vector, the commutation process finishes.

During the commutation interval, the voltage vectors [010] and [110] are applied alternately. That means phase A is modulated, and the upper switch of phase B and lower switch of phase C are both ON. So, $u_{\mathrm{BCI}} = u_{\mathrm{dc}}$ and $u_{\mathrm{CCI}} = 0$ are obtained. Then, the output voltage of every phase can be calculated as

$$u_{\mathrm{ACI}} = (d_{\mathrm{NC}} + 0.5)u_{\mathrm{dc}} - 0.5Ri_{\mathrm{ACS}}, u_{\mathrm{BCI}} = u_{\mathrm{dc}}, u_{\mathrm{CCI}} = 0. \tag{19}$$

The detailed calculation process of u_{ACI} can be found in Appendix A. Taking $u_{\alpha \mathrm{CI}} = e_{\alpha \mathrm{CI}} + Ri_{\alpha \mathrm{CS}}$, $u_{\beta \mathrm{CI}} = \sqrt{1/2}u_{\mathrm{dc}}$ and (8) into (13), the commutation time of LS_RCTR can be calculated as

$$t_{\mathrm{com}} \approx \frac{2i_{\mathrm{ACS}}L}{u_{\mathrm{dc}} + Ri_{\mathrm{ACS}}}. \tag{20}$$

B. HS_RCTR

As shown in Fig. 4(b), at high-speed operation, $|e_{\alpha \mathrm{CI}} + Ri_{\alpha \mathrm{CS}}| > \sqrt{1/6}u_{\mathrm{dc}}$, to RCTR, $u_{\alpha \mathrm{CI}} = e_{\alpha \mathrm{CI}} + Ri_{\alpha \mathrm{CS}}$ should be satisfied. $u_{\beta \mathrm{CI}}$ should be as large as possible to short commutation time. Thus, *B* is selected as the work point. Its coordinate can be expressed as

$$u_{\alpha \mathrm{CI}} + ju_{\beta \mathrm{CI}} = \sqrt{2/3}d_{\mathrm{NC}}u_{\mathrm{dc}} + (\sqrt{3/2} - 2\sqrt{2/3})Ri_{\mathrm{ACS}} + j\sqrt{2}(1 - d_{\mathrm{NC}})u_{\mathrm{dc}}. \tag{21}$$

It can be seen from Fig. 4(b) that the output vector corresponding to point B is obtained by the linear combination of vector [100] and [110], so $u_{\mathrm{ACI}} = u_{\mathrm{dc}}$ and $u_{\mathrm{CCI}} = 0$. Then, the output voltage of every phase can be calculated as

$$u_{\mathrm{ACI}} = u_{\mathrm{dc}}, u_{\mathrm{BCI}} = (2 - 2d_{\mathrm{NC}})u_{\mathrm{dc}} + Ri_{\mathrm{ACS}}, u_{\mathrm{CCI}} = 0. \tag{22}$$

Taking $u_{\alpha \mathrm{CI}} = e_{\alpha \mathrm{CI}} + Ri_{\alpha \mathrm{CS}}$, $u_{\beta \mathrm{CI}} = \sqrt{2}(1 - d_{\mathrm{NC}})u_{\mathrm{dc}}$, and (8) into (13), the commutation time of LS_RCTR can be calculated as

$$t_{\mathrm{com}} \approx \frac{i_{\mathrm{ACS}}L}{(1 - d_{\mathrm{NC}})u_{\mathrm{dc}} + 0.5Ri_{\mathrm{ACS}}}. \tag{23}$$

C. Shortcoming of RCTR

When d_{NC} is very close to 1, it should be noted that the commutation time is very long from (23) when HS_RCTR is used. When the commutation time is longer than the time corresponding to 30 electrical degrees, commutation failure will take place. It will cause phase current increase sharply, and a large torque

fluctuation will be also presented, even causing over-current protection.

So, when the motor operates in a high-speed and heavy load condition, RCT should take precedence over RCTR to avoid commutation failure.

IV. Reduce Commutation Torque

A. LS_RCT

Equation (13) indicates that, increasing $u_{\beta\mathrm{CI}}$ or decreasing $u_{\alpha\mathrm{CI}}$ will reduce the commutation time. At low-speed operation, when the work point locates A, the only way to reduce the commutation time is to decrease $u_{\alpha\mathrm{CI}}$, because $u_{\beta\mathrm{CI}}$ cannot be magnified. In this case, the work point should move from point A to point A1 as shown in Fig. 4(a), where $u_{\alpha\mathrm{CI}}$ decreases but $u_{\beta\mathrm{CI}}$ keeps maximum, and the corresponding coordinate of A1 can be expressed as

$$\begin{cases} -\sqrt{1/6}u_{\mathrm{dc}} < u_{\alpha\mathrm{CI}} < e_{\alpha\mathrm{CI}} + Ri_{\alpha\mathrm{CS}} \\ u_{\beta\mathrm{CI}} = \sqrt{1/2}u_{\mathrm{dc}} \end{cases}. \tag{24}$$

In fact, the exact coordinate of A1 should be determined by preset commutation time.

Taking (24) into (13) and (15), the commutation time and the NCP current at the end of the commutation can be calculated as

$$t_{\mathrm{com}} \approx \frac{i_{\mathrm{ACS}}L}{(\frac{1}{2}+\frac{1}{3}d_{\mathrm{NC}})u_{\mathrm{dc}} - \sqrt{\frac{1}{6}}u_{\alpha\mathrm{CI}} + \frac{1}{3}Ri_{\mathrm{ACS}}} \tag{25}$$

$$i_{\mathrm{ACE}} = -i_{\mathrm{CCE}} \approx \frac{i_{\mathrm{ACS}}\left((3-2d_{\mathrm{NC}})u_{\mathrm{dc}} + \sqrt{6}u_{\alpha\mathrm{CI}} + 4Ri_{\mathrm{ACS}}\right)}{(3+2d_{\mathrm{NC}})u_{\mathrm{dc}} - \sqrt{6}u_{\alpha\mathrm{CI}} + 2Ri_{\mathrm{ACS}}}. \tag{26}$$

It can be seen that during commutation interval, the NCP current has a fluctuation while LS_RCT is applied.

Similar to the derivation of (19), the output voltage of every phase can be calculated as

$$u_{\mathrm{ACI}} = \sqrt{3/2}u_{\alpha\mathrm{CI}} + 0.5u_{\mathrm{dc}}, u_{\mathrm{BCI}} = u_{\mathrm{dc}}, u_{\mathrm{CCI}} = 0. \tag{27}$$

Fig. 5 shows the PWM sequences of LS_RCTR and LS_RCT. The gray area represents the current flows through the fly-wheel diode of the corresponding switch.

B. HS_RCT1

At high-speed operation, when the VSI operates at work point B as shown in Fig. 4(b), to reduce the commutation time, we can increase $u_{\beta\mathrm{CI}}$ and/or decrease $u_{\alpha\mathrm{CI}}$. Then, the work point can move from B to B1 or B2. When it moves to B1, voltage vectors [100] and [110] are applied. When it moves to B2, voltage vectors [110] and [010] are applied and shorter commutation time is obtained. Distinguishing the two cases, the control to RCT is named HS_RCT1 and HS_RCT2, respectively.

Under HS_RCT1, $u_{\alpha\mathrm{CI}}$ is decreased and $u_{\beta\mathrm{CI}}$ is increased to RCT. The coordinates of B1 can be expressed as

$$\begin{cases} \sqrt{1/6}u_{\mathrm{dc}} < u_{\alpha\mathrm{CI}} < e_{\alpha\mathrm{CI}} + Ri_{\alpha\mathrm{CS}} \\ u_{\beta\mathrm{CI}} = \sqrt{2}u_{\mathrm{dc}} - \sqrt{3}u_{\alpha\mathrm{CI}} \end{cases}. \tag{28}$$

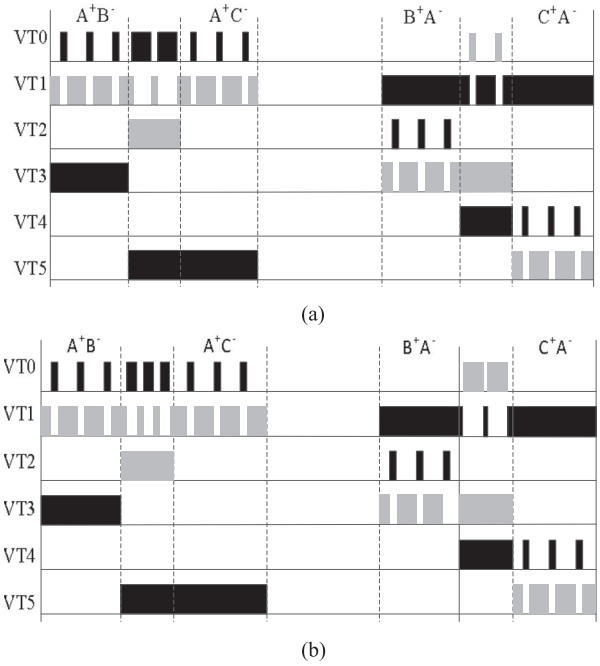

Fig. 5. Commutation control at low-speed operation. (a) LS_RCTR. (b) LS_RCT.

Taking (28) into (13) and (15), the commutation time and the NCP current at the end of the commutation can be calculated as

$$t_{\mathrm{com}} \approx \frac{i_{\mathrm{ACS}}L}{(1+\frac{d_{\mathrm{NC}}}{3})u_{\mathrm{dc}} - 2\sqrt{\frac{2}{3}}u_{\alpha\mathrm{CI}} + \frac{1}{3}Ri_{\mathrm{ACS}}} \tag{29}$$

$$i_{\mathrm{ACE}} \approx \frac{(3-d_{\mathrm{NC}})u_{\mathrm{dc}} - \sqrt{6}u_{\alpha\mathrm{CI}}}{(3+d_{\mathrm{NC}})u_{\mathrm{dc}} - 2\sqrt{6}u_{\alpha\mathrm{CI}} + Ri_{\mathrm{ACS}}} i_{\mathrm{ACS}} < i_{\mathrm{ACS}}. \tag{30}$$

It also can be seen that there is a fluctuation on the NCP current during commutation interval.

The output voltage of every phase can be calculated as

$$u_{\mathrm{ACI}} = u_{\mathrm{dc}}, u_{\mathrm{BCI}} = 2u_{\mathrm{dc}} - \sqrt{6}u_{\alpha\mathrm{CI}}, u_{\mathrm{CCI}} = 0. \tag{31}$$

C. HS_RCT2

Under HS_RCT2, $u_{\alpha\mathrm{CI}}$ is decreased and $u_{\beta\mathrm{CI}}$ maintains maximum to reduce the commutation time. The coordinates of B2 can be obtained as

$$\begin{cases} -\sqrt{1/6}u_{\mathrm{dc}} < u_{\alpha\mathrm{CI}} < \sqrt{1/6}u_{\mathrm{dc}} \\ u_{\beta\mathrm{CI}} = \sqrt{1/2}u_{\mathrm{dc}} \end{cases}. \tag{32}$$

Taking (32) into (13) and (15), the commutation time and the NCP current at the end of the commutation can be calculated as

$$t_{\mathrm{com}} \approx \frac{i_{\mathrm{ACS}}L}{(\frac{1}{2}+\frac{1}{3}d_{\mathrm{NC}})u_{\mathrm{dc}} - \sqrt{\frac{1}{6}}u_{\alpha\mathrm{CI}} + \frac{1}{3}Ri_{\mathrm{ACS}}} \tag{33}$$

$$i_{\mathrm{ACE}} \approx i_{\mathrm{ACS}}\frac{(3-2d_{\mathrm{NC}})u_{\mathrm{dc}} + \sqrt{6}u_{\alpha\mathrm{CI}}}{(3+2d_{\mathrm{NC}})u_{\mathrm{dc}} - \sqrt{6}u_{\alpha\mathrm{CI}} + Ri_{\mathrm{ACS}}} < i_{\mathrm{ACS}}. \tag{34}$$

The output voltage of every phase can be calculated as

$$u_{\mathrm{ACI}} = \sqrt{3/2}u_{\alpha\mathrm{CI}} + \frac{u_{\mathrm{dc}}}{2}, u_{\mathrm{BCI}} = u_{\mathrm{dc}}, u_{\mathrm{CCI}} = 0. \tag{35}$$

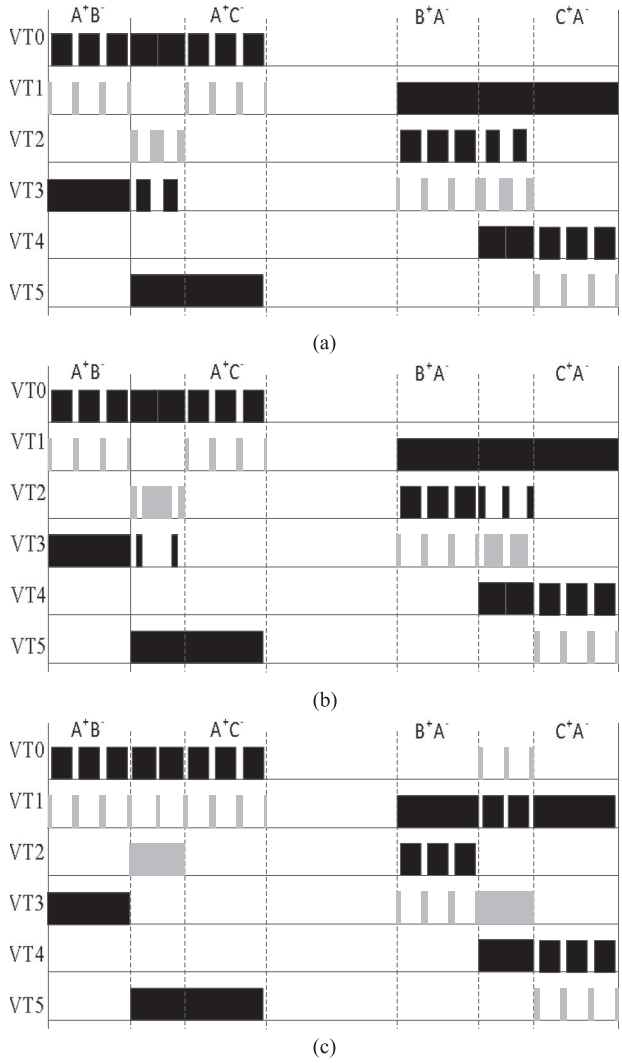

Fig. 6. Commutation control at high-speed operation. (a) HS_RCTR. (b) HS_RCT1. (c) HS_RCT2.

Fig. 6 shows the PWM sequences of HS_RCTR, HS_RCT1, and HS_RCT2, where the gray area represents the current flows through the fly-wheel diode of the corresponding switch.

V. Hybrid Control of RCTR and RCT

With the increase of d_{NC} and the NCP current at the beginning of the commutation, the commutation time becomes longer. Commutation failure may take place when LS_RCTR and HS_RCTR are used to reduce the commutation torque ripple. Thus, RCT should take precedence over RCTR. To realize hybrid control, if the commutation time calculated by (20) and (23) is longer than the time corresponding to 15 electrical degrees, RCT should be adopted other than RCTR. Assuming ω denotes the angular velocity, and then the time corresponding to 15 electrical degrees can be given as

$$t_{\mathrm{cri}} = \frac{\pi}{12\omega}. \tag{36}$$

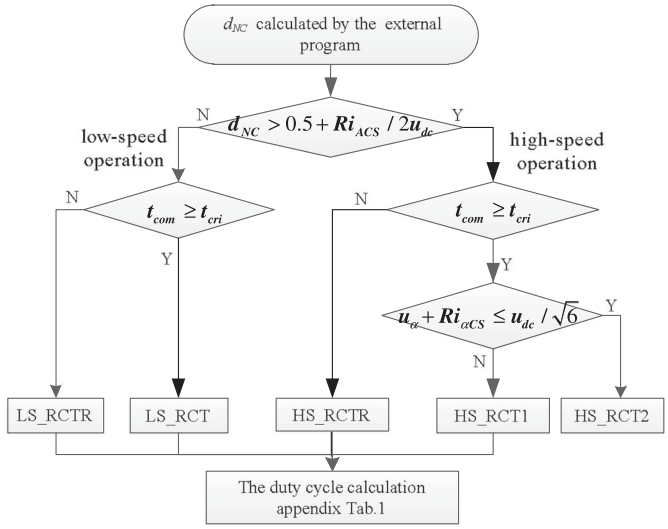

Fig. 7. Flowchart of the hybrid control of RCTR and RCT.

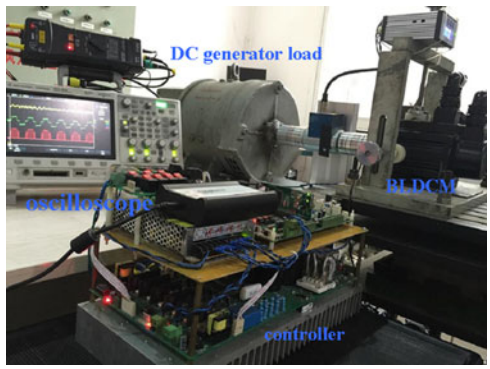

Fig. 8. Hardware experimental platform.

TABLE II
Experimental Parameters

Rated power (W)	780
DC-link voltage (V)	110
Rated current (A)	10
Rated torque (N·m)	15
Phase inductance (mH)	2.2
Phase resistance (Ω)	0.15
Rated speed (r/min)	2500
Pairs of poles	2

As mentioned before, when $d_{\mathrm{NC}} \leq 0.5 + Ri_{\mathrm{ACS}}/2u_{\mathrm{dc}}$, the BLDCM works at low-speed operation. If $t_{\mathrm{com}} > t_{\mathrm{cri}}$, LS_RCT should be used. From (24) and (25), the work point of VSI under LS_RCT is

$$\begin{cases} u_{\alpha \mathrm{CI}} = \sqrt{3/2}u_{\mathrm{dc}} + \sqrt{2/3}d_{\mathrm{NC}}u_{\mathrm{dc}} + \sqrt{6}Ri_{\mathrm{ACS}} - \dfrac{\sqrt{6}i_{\mathrm{ACS}}L}{t_{\mathrm{cri}}} \\ u_{\beta \mathrm{CI}} = \sqrt{1/2}u_{\mathrm{dc}} \end{cases}. \tag{37}$$

When $\boldsymbol{d}_{\mathrm{NC}} > 0.5 + \boldsymbol{Ri}_{\mathrm{ACS}}/2\boldsymbol{u}_{\mathrm{dc}}$, the BLDCM works at high-speed operation. If $t_{\mathrm{com}} > t_{\mathrm{cri}}$, HS_RCT1 or HS_RCT2 should be used. From (28) and (29), the work point of VSI under

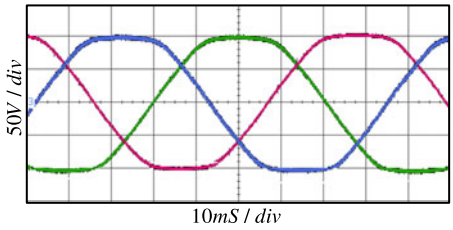

Fig. 9. Measured EMF of BLDCM.

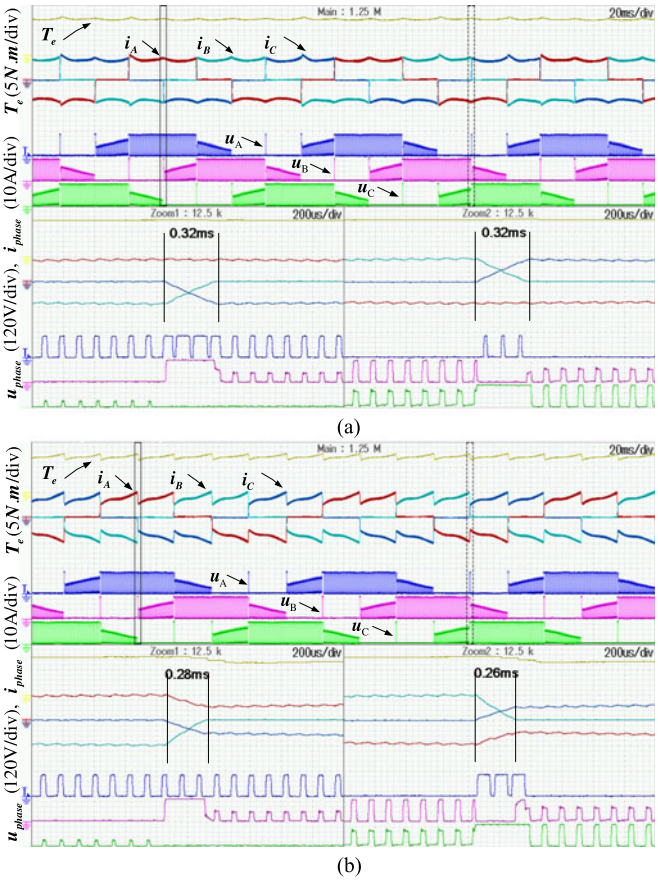

Fig.10. Experimental results at low-speed operation. (a) LS_RCTR. (b) LS_RCT.

TABLE III
THEORETICAL AND PRACTICAL VALUES OF t_{COM} AND i_{ACE}

		Theoretical values $t_{\mathrm{com}}(\mathrm{ms})i_{\mathrm{ACE}}(\mathrm{A})$		Practical values $t_{\mathrm{com}}(\mathrm{ms})i_{\mathrm{ACE}}(\mathrm{A})$	
Low-speed operation					
LS_RCTR	USC	0.32	−10	0.32	−9.8
	LSC	0.32	10	0.32	10.2
LS_RCT	USC	0.25	−3.63	0.26	−4.92
	LSC	0.25	3.63	0.28	4.9
High-speed operation					
HS_RCTR	USC	0.54	−10	0.56	−10.2
	LSC	0.54	10	0.58	10
HS_RCT1	USC	0.43	−8.78	0.45	−9.4
	LSC	0.44	8.78	0.47	9.6
HS_RCT2	USC	0.37	−6.82	0.40	−7.4
	LSC	0.34	6.82	0.40	7.2

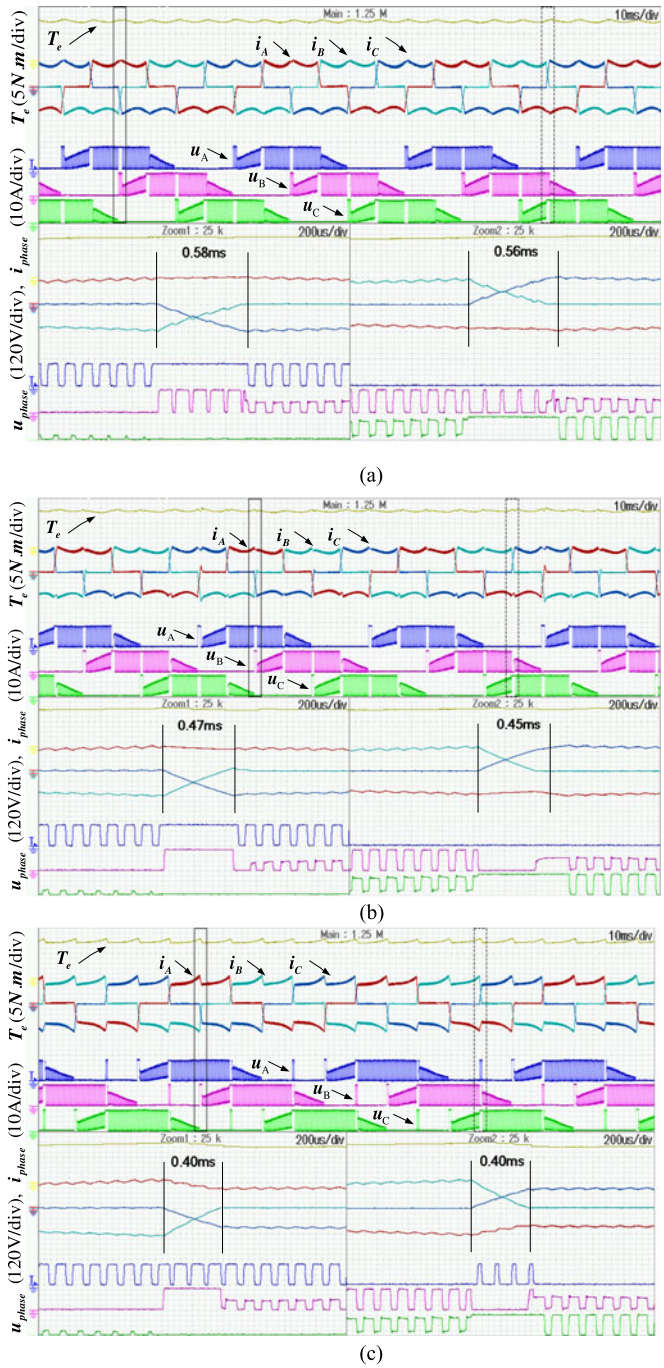

Fig. 11. Experimental results at high-speed operation. (a) HS_RCTR. (b) HS_RCT1. (c) HS_RCT2.

HS_RCT1 is

$$\begin{cases} u_{\alpha\mathrm{CI}} = \sqrt{3/8}u_{\mathrm{dc}} + \sqrt{1/24}d_{\mathrm{CN}}u_{\mathrm{dc}} + \sqrt{3/8}Ri_{\mathrm{ACS}} \\ \quad -\sqrt{3/8}\dfrac{i_{\mathrm{ACS}}L}{t_{\mathrm{cri}}} \\ u_{\beta\mathrm{CI}} = \sqrt{1/8}\left(u_{\mathrm{dc}} - d_{\mathrm{CN}}u_{\mathrm{dc}} + 3\dfrac{i_{\mathrm{ACS}}L}{t_{\mathrm{cri}}}\right) \end{cases}. \quad (38)$$

From Fig. 4(b), it can be seen that when $u_\alpha + Ri_{\alpha\mathrm{CS}} > u_{\mathrm{dc}}/\sqrt{6}$, HS_RCT1 should be applied; otherwise, HS_RCT2

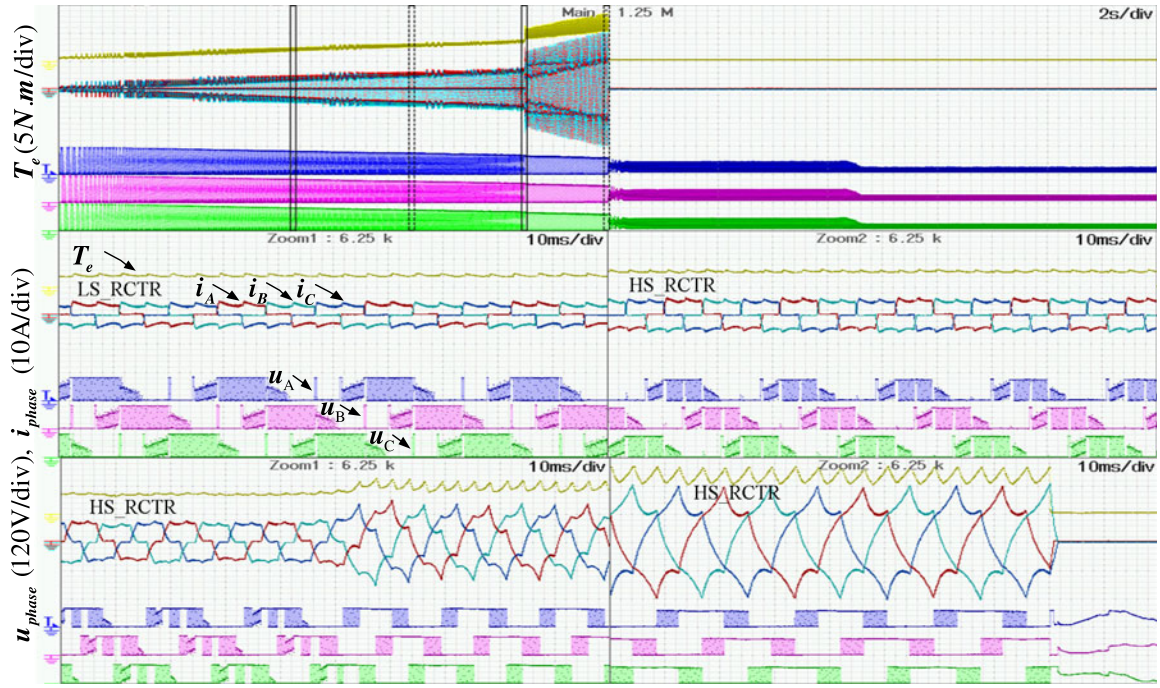

Fig. 12. Dynamic experimental results under RCTR.

should be used. According to (32) and (33), the work point of VSI under HS_RCT2 is

$$\begin{cases} u_{\alpha \mathrm{CI}} = \sqrt{3/2}u_{\mathrm{dc}} + \sqrt{2/3}d_{\mathrm{NC}}u_{\mathrm{dc}} + \sqrt{6}Ri_{\mathrm{ACS}} - \dfrac{\sqrt{6}i_{\mathrm{ACS}}L}{t_{\mathrm{cri}}} \\ u_{\beta \mathrm{CI}} = \sqrt{1/2}u_{\mathrm{dc}} \end{cases}. \tag{39}$$

Fig. 7 shows the flowchart of hybrid control of RCTR and RCT. The table in Appendix B gives the phase voltage under the different control modes during the commutation interval, where u_{NCP}, u_{OGP}, and u_{ICP} represent the voltage of the NCP, OGP, and ICP, respectively.

VI. Experimental Verification

In order to verify the proposed method, the experimental setup of a BLDCM connected with a dc generator load is shown in Fig. 8. A MC56F8037 DSP is chosen as the control chip. Table II shows the experimental parameters. The measured EMF of the BLDCM is shown in Fig. 9.

A. Experiments of Independent Operation Modes

Figs. 10 and 11 show the experimental results of the BLDCM at low-speed operation and high-speed operation under the different commutation control modes. The NCP current is 10 A at the beginning of the commutation. The top of each figure shows multicycle waveforms, and the commutation process are further shown at the bottom, where the commutation from A^+B^- to A^+C^- and from B^+A^- to C^+A^- are taken as examples of the commutation between the LSC and USC, respectively.

Fig. 10 shows the experimental results under LS_RCTR and LS_RCT. The current slew rate of the OGP is roughly equal to that of the ICP, and the NCP current does not obviously vary during the commutation interval under LS_RCTR. But the NCP current is reduced to about 4.9 A at the end of the commutation under LS_RCT. The commutation time is 0.32 ms under LS_RCTR compared with 0.28 ms under LS_RCT.

Table III shows the theoretical values and practical values of the commutation time and the NCP current at the end of the commutation. The theoretical values of the commutation times are calculated by (23), (26), (28), (32), and (36), respectively, which assume that the EMFs of the BLDCM keep consistent during commutation interval.

Fig. 11 shows the experimental results under HS_RCTR, HS_RCT1, and HS_RCT2. The current slew rate of the OGP is roughly equal to that of the ICP, and the NCP current does not obviously vary during the commutation interval under HS_RCTR. The current slew rate of the OGP is greater than that of the ICP, and the NCP current is reduced to about 9.4 and 8.2 A at the end of the commutation under HS_RCT1 and HS_RCT2, respectively. The commutation time under HS_RCTR, HS_RCT1, and HS_RCT2 is about 0.56, 0.46, and 0.4 ms, respectively. Table III shows the theoretical values and practical values of the commutation time and the NCP current at the end of the commutation.

It can be seen that, whether at high-speed operation or low-speed operation, in order to shorten commutation time to avoid commutation failure, RCT is an effective way, although it will sacrifice the quality of torque during the commutation interval.

B. Dynamic Experiment

The dynamic experiment is carried out to illustrate the effectiveness of the hybrid control of RCTR and RCT. The duty

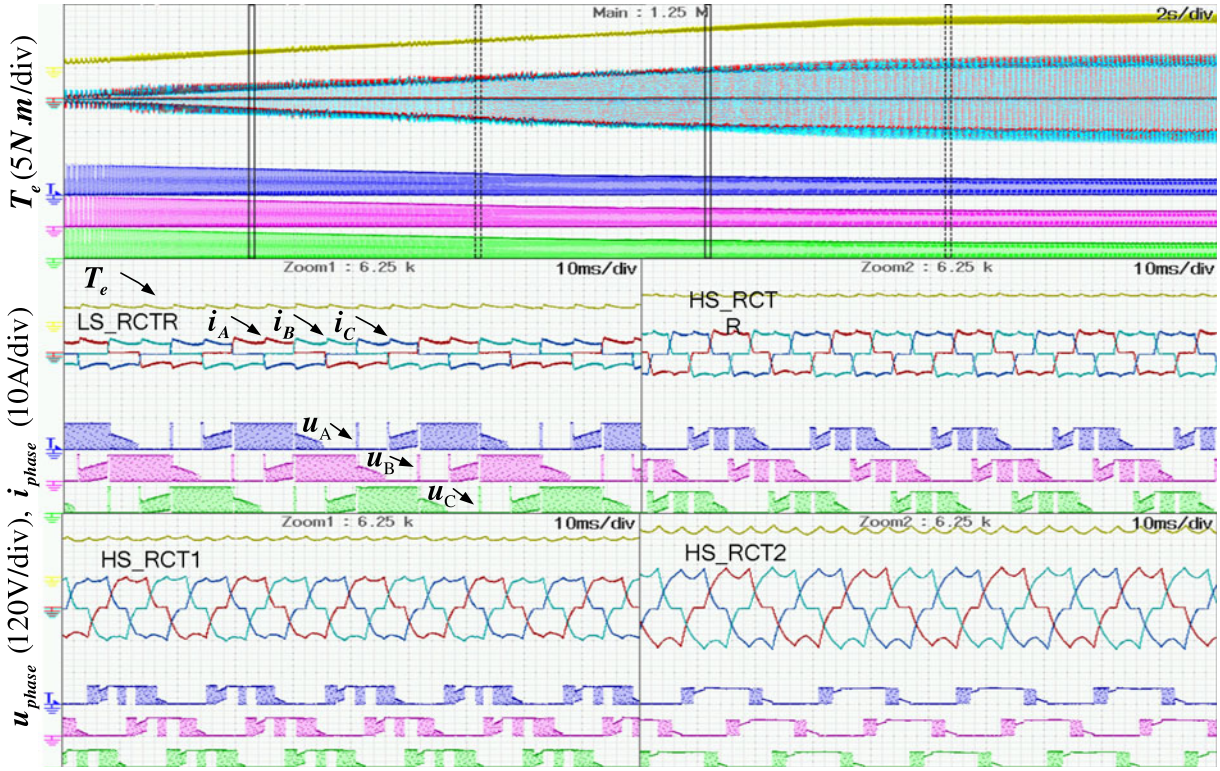

Fig. 13. Dynamic experimental results under the hybrid commutation control.

cycle d_{NC} is increased from 0% to 100%. A dc generator with the rated field excitation is adopted as the load, so the outputted voltage is proportional to the motor speed. The top of each figure shows the full range waveforms, and the waveforms under different modes are further shown at the bottom.

Fig. 12 shows the experiment result of using only LS_RCTR and HS_RCTR to reduce the commutation torque ripple. It can be seen from Fig. 12 that with the increase of the duty cycle, the motor current increases, and the commutation time becomes longer. It should be noted that the dc-link voltage decreases continuously, that is because a storage battery is adopted as the dc source. Therefore, with the increase of the duty cycle, the actual speed may decrease when the dc-link voltage decreases to a certain value. As can be seen from Fig. 12, LS_RCTR is used when the duty cycle is less than 50%, so that commutation failure does not occur; HS_RCTR is used when the duty cycle is greater than 50%. When the duty cycle increases to about 75%, commutation failure takes place. The phase currents of the BLDCM increase rapidly, and then the motor stops working due to over-current protection.

Fig. 13 is the experimental result of hybrid control of RCTR and RCT. LS_RCTR is used when the duty cycle is less than 50%. HS_RCTR is used when the duty cycle is greater than 50% (about 50%–75%). In order to avoid commutation failure, HS_RCT1 is used when the duty cycle is greater than about 75% (about 75%–90%) and HS_RCT2 is used when the duty cycle is greater than about 90% (about 90%–100%), where although commutation torque ripple arises, commutation failure does not occur. It can be seen that the hybrid commutation control method proposed in this paper can ensure that the motor operates in full speed range.

VII. Conclusion

To simplify commutation analysis of BLDCM, a novel analysis method based on Clarke transformation is proposed. Based on the method, commutation control of RCTR and RCT are deduced in this paper.

The proposed commutation control is a compromise between RCTR and RCT. Compared with the traditional method, the presented method has the following advantages.

1) The complex circuit analyses are avoided during the commutation interval.
2) RCTR and RCT are coordinated to make the motor operate with good performances in full speed range.
3) The presented method is easy to implement. It is only required to change the software instead of hardware.

Appendix

The output voltage of every phase can be calculated as follows.

When the output vector of the VSI is obtained by linear combination of voltage vectors [010] and [110], that means $u_{\mathrm{BCI}} = u_{\mathrm{dc}}$ and $u_{\mathrm{CCI}} = 0$. According to Clarke transformation, we can get

$$u_{\alpha\mathrm{CI}} = \sqrt{2/3}\left(u_{\mathrm{ACI}} - \frac{u_{\mathrm{BCI}}}{2} - \frac{u_{\mathrm{CCI}}}{2}\right) \Rightarrow u_{\mathrm{ACI}} = \sqrt{3/2}\,u_{\alpha\mathrm{CI}} + \frac{u_{\mathrm{dc}}}{2}. \tag{A1}$$

When the output vector of the VSI is obtained by linear combination of voltage vectors [100] and [110], that means $u_{\mathrm{ACI}} = u_{\mathrm{dc}}$ and $u_{\mathrm{CCI}} = 0$. Similarly, we can get

$$u_{\alpha\mathrm{CI}} = \sqrt{2/3}\left(u_{\mathrm{ACI}} - \frac{u_{\mathrm{BCI}}}{2} - \frac{u_{\mathrm{CCI}}}{2}\right) \Rightarrow u_{\mathrm{BCI}} = 2u_{\mathrm{dc}} - \sqrt{6}u_{\alpha\mathrm{CI}}. \tag{A2}$$

TABLE AI
PHASE VOLTAGES UNDER DIFFERENT COMMUTATION CONTROL MODES

Operating mode	Commutation between LSC	Commutation between USC
LS_RCTR	$u_{\mathrm{NCP}} = (d_{\mathrm{NC}} + 0.5)$ $u_{\mathrm{dc}} - 0.5Ri_{\mathrm{ACS}}$ $u_{\mathrm{OGP}} = u_{\mathrm{dc}}$ $u_{\mathrm{ICP}} = 0$	$u_{\mathrm{NCP}} = (0.5 - d_{\mathrm{NC}})$ $u_{\mathrm{dc}} + 0.5Ri_{\mathrm{ACS}}$ $u_{\mathrm{OGP}} = 0$ $u_{\mathrm{ICP}} = u_{\mathrm{dc}}$
LS_RCT	$u_{\mathrm{NCP}} = \sqrt{3/2}u_{\alpha}$ $+ 0.5u_{\mathrm{dc}}$ $u_{\mathrm{OGP}} = u_{\mathrm{dc}}$ $u_{\mathrm{ICP}} = 0$	$u_{\mathrm{NCP}} = -\sqrt{3/2}u_{\alpha}$ $+ 0.5u_{\mathrm{dc}}$ $u_{\mathrm{OGP}} = 0$ $u_{\mathrm{ICP}} = u_{\mathrm{dc}}$
HS_RCTR	$u_{\mathrm{NCP}} = u_{\mathrm{dc}}$ $u_{\mathrm{OGP}} = 2(1 - d_{\mathrm{NC}})u_{\mathrm{dc}}$ $+ Ri_{\mathrm{ACS}}$ $u_{\mathrm{ICP}} = 0$	$u_{\mathrm{NCP}} = 0$ $u_{\mathrm{OGP}} = (2d_{\mathrm{NC}} - 1)u_{\mathrm{dc}}$ $-Ri_{\mathrm{ACS}}$ $u_{\mathrm{ICP}} = u_{\mathrm{dc}}$
HS_RCT1	$u_{\mathrm{NCP}} = u_{\mathrm{dc}}$ $u_{\mathrm{OGP}} = 2u_{\mathrm{dc}} - \sqrt{6}u_{\alpha}$ $u_{\mathrm{ICP}} = 0$	$u_{\mathrm{NCP}} = 0$ $u_{\mathrm{OGP}} = \sqrt{6}u_{\alpha} - u_{\mathrm{dc}}$ $u_{\mathrm{ICP}} = u_{\mathrm{dc}}$
HS_RCT2	$u_{\mathrm{NCP}} = \sqrt{3/2}u_{\alpha}$ $+ 0.5u_{\mathrm{dc}}$ $u_{\mathrm{OGP}} = u_{\mathrm{dc}}$ $u_{\mathrm{ICP}} = 0$	$u_{\mathrm{NCP}} = -\sqrt{3/2}u_{\alpha}$ $+ 0.5u_{\mathrm{dc}}$ $u_{\mathrm{OGP}} = 0$ $u_{\mathrm{ICP}} = u_{\mathrm{dc}}$

REFERENCES

[1] C. L. Xia, "*Permanent Magnet Brushless DC Motor Drives and Controls*," Hoboken, NJ, USA: Wiley, 2012.

[2] X. Huang, A. Goodman, C. Gerada, Y. Fang, and Q. Lu, "A single sided matrix converter drive for a brushless DC motor in aerospace applications," *IEEE Trans. Ind. Electron.*, vol. 59, no. 9, pp. 3542–3552, Sep. 2012.

[3] T. K. A. Brekken, H. M. Hapke, C. Stillinger, and J. Prudell, "Machines and drives comparison for low-power renewable energy and oscillating applications," *IEEE Trans. Energy Convers.*, vol. 25, no. 4, pp. 1162–1170, Dec. 2010.

[4] J. Fang, H. Li, and B. Han, "Torque ripple reduction in BLDC torque motor with non-ideal back EMF," *IEEE Trans. Power Electron.*, vol. 27, no. 11, pp. 4630–4637, Nov. 2012.

[5] W. Li, J. Fang, H. Li, and J. Tang, "Position sensorless control without phase shifter for high-speed BLDC motors with low inductance and non-ideal back EMF," *IEEE Trans. Power Electron.*, vol. 31, no. 2, pp. 1354–1366, Feb. 2016.

[6] T. Sheng, X. Wang, J. Zhang, and Z. Deng, "Torque-ripple mitigation for brushless DC machine drive system using one-cycle average torque control," *IEEE Trans. Ind. Electron.*, vol. 62, no. 4, pp. 2114–2122, Apr. 2015.

[7] R. Carlson, M. Lajoie-Mazenc, and J. C. D. S. Fagundes, "Analysis of torque ripple due to phase commutation in brushless dc machines," *IEEE Trans. Ind. Appl.*, vol. 28, no. 3, pp. 632–638, May/Jun. 1992.

[8] T. M. Jahns and W. I. Soong, "Pulsating torque minimization techniques for permanent magnet AC motor drives-a review," *IEEE Trans. Ind. Electron.*, vol. 43, no. 2, pp. 321–330, Apr. 1996.

[9] Y. K. Lin and Y. S. Lai, "Pulse width modulation technique for BLDCM drives to reduce commutation torque ripple without calculation of commutation time," *IEEE Trans. Ind. Appl.*, vol. 47, no. 4, pp. 1786–1793, Jul./Aug. 2011.

[10] J. H. Song and I. Choy, "Commutation torque ripple reduction in brushless dc motor drives using a single dc current sensor," *IEEE Trans. Power Electron.*, vol. 19, no. 2, pp. 312–319, Mar. 2004.

[11] H. Lu, L. Zhang, and W. Qu, "A new torque control method for torque ripple minimization of BLDC motors with un-ideal back EMF," *IEEE Trans. Power Electron.*, vol. 23, no. 2, pp. 950–958, Mar. 2008.

[12] D.-K. Kim, K.-W. Lee, and B.-I. Kwon, "Commutation torque ripple reduction in a position sensorless brushless dc motor drive," *IEEE Trans. Power Electron.*, vol. 21, no. 6, pp. 1762–1768, Nov. 2006.

[13] J. Shi and T. Li, "New method to eliminate commutation torque ripple of brushless DC motor with minimum commutation time," *IEEE Trans. Ind. Electron.*, vol. 60, no. 6, pp. 2139–2146, Jun. 2013.

[14] C. L. Xia, Y. F. Wang, and T. N. Shi, "Implementation of finite-state model predictive control for commutation torque ripple minimization of permanent-magnet brushless DC motor," *IEEE Trans. Ind. Electron.*, vol. 60, no. 3, pp. 896–905, Mar. 2013.

[15] X. F. Zhang, Q. B. Hu, and Z. Y. Lu, "Torque ripple reduction in brushless dc motor drives using a buck converter," *Trans. China Electrotech. Soc.*, vol. 20, no. 9, pp. 72–81, Sep. 2005.

[16] K. Y. Nam, W. T. Lee, C. M. Lee, and J. P. Hong, "Reducing torque ripple of brushless dc motor by varying input voltage," *IEEE Trans. Magn.*, vol. 42, no. 4, pp. 1307–1310, Apr. 2006.

[17] T. Shi, Y. Guo, P. Song, and C. Xia, "A new approach of minimizing commutation torque ripple for brushless dc motor based on dc-dc converter," *IEEE Trans. Ind. Electron.*, vol. 57, no. 10, pp. 3483–3490, Oct. 2010.

[18] V. Viswanathan and S. Jeevananthan, "Approach for torque ripple reduction for brushless DC motor based on three-level neutral-point-clamped inverter with DC–DC converter," *IET Power Electron.*, vol. 8, no. 1, pp. 47–55, Jan. 2015.

[19] V. Bist and B. Singh, "Reduced sensor configuration of brushless DC motor drive using a power factor correction-based modified-zeta converter," *IET Power Electron.*, vol. 7, no. 9, pp. 2322–2335, Sep. 2014.

[20] X. Li, C. Xia, Y. Cao, W. Chen, and T. Shi, "Commutation torque ripple reduction strategy of Z-source inverter fed brushless DC motor," *IEEE Trans. Power Electron.*, vol. 31, no. 11, pp. 7677–7690, Nov. 2016.

[21] G. Buja, M. Bertoluzzo, and R. K. Keshri, "Torque ripple-free operation of PM BLDC drives with petal-wave current supply," *IEEE Trans. Ind. Electron.*, vol. 62, no. 7, pp. 4034–4043, Jul. 2015.

[22] Q. Han, N. Samoylenko, and J. Jatskevich, "Average-value modeling of brushless DC motors with 120 voltage source inverter," *IEEE Trans. Energy Convers.*, vol. 23, no. 2, pp. 423–432, Jun. 2008.

[23] Z. Q. Zhu, J. D. Ede, and D. Howe, "Design criteria for brushless DC motors for high-speed sensorless operation," *Int. J. Appl. Electromagn. Mech.*, vol. 15, no. 1–4, pp. 79–87, 2001.

[24] Y. Wei, Y. Xu, J. Zou, and H. Wang, "Analytic investigation on commutation angle of brushless DC motors with 120 voltage source inverter," *Int. J. Appl. Electromagn. Mech.*, vol. 45, no. 1–4, pp. 219–225, 2014.

[25] H. Li, S. Zheng, and H. Ren, "Self-correction of commutation point for high-speed sensorless BLDC motor with low inductance and non-ideal back EMF," *IEEE Trans. Power Electron.*, vol. 32, no. 1, pp. 642–651, Jan. 2017, doi 10.1109/TPEL.2016.2524632.

[26] Y. Liu, Z. Q. Zhu, and D. Howe, "Commutation-torque-ripple minimization in direct-torque-controlled PM brushless dc drives," *IEEE Trans. Ind. Appl.*, vol. 43, no. 4, pp. 1012–1021, Jul./Aug. 2007.

[27] P. Lin, K. Wei, and Z. C. Zhang, "A novel control scheme to suppress the commutation torque ripple in BLDCM," *Proc. Chin. Soc. Elect. Eng.*, vol. 26, no. 3, pp. 153–158, Feb. 2006.

[28] "Approach for torque ripple reduction for brushless DC motor based on three-level neutral-point-clamped inverter with DC-DC converter," *IET Power Electron.*, vol. 8, no. 1, pp. 47–55. 2015.

Weidong Jiang (M'15) was born in Sichuan, China, in 1976. He received the B.S. and Ph.D degrees in electrical engineering. from Hefei university of Technology, Hefei, China, in1999 and 2004, respectively.

Since June 2004, he has been in the School of Electrical Engineering and Automation, Hefei University of Technology, Hefei, China, where he is currently a Professor. His research interests include electrical machines and their control systems, power electronics, and electric drives.

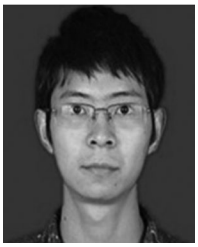

Yuming Liao was born in Ganzhou, Jiangxi Province, China, in 1994. He received the B.S. degree in electrical engineering and automation from the Department of Electrical Engineering and Automation, Nanchang Institute of Technology, Nanchang, China, in 2015. He is working toward the M.S. degree in electronics and power transmission from the Department of Electrical Engineering, Hefei university of Technology, Hefei, China.

His research interests include electrical machines and motor drives, power electronics.

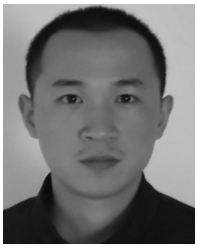

Jinping Wang was born in Hunan, China, in 1984. He received the B.S. degree in electronic and information engineering and the Ph.D. degree in electrical engineering from Southwest Jiaotong University, Chengdu, China, in 2007 and 2013.

Since June 2013, he has been in the School of Electrical Engineering and Automation, Hefei University of Technology, Hefei, China, where he is currently an Associate Professor. His main research interests include modeling, analysis, control, and applications of switching-mode power supplies.

Peixia Wang was born in Anhui, China, in 1991. She received the B.S. degree in electrical engineering and automation from the Department of Electrical Engineering, Anhui Polytechnic University, Wuhu, China, in 2015. She is working toward the M.S. degree in electronics and power transmission from Department of Information Engineering, Hefei university of Technology Xuancheng Campus, Xuancheng, China.

Her main research interests include power electronics, and power converters in renewable energy.

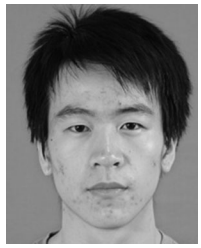

Yifan Xie was born in Changzhou, Jiangsu Province, China, in 1993. He is currently working toward the B.S. degree in electrical engineering and automation from the Department of Electrical Engineering, Hefei university of Technology, Hefei, China.

His research interests include application of power converters in renewable energy and power quality.